REMIGRATION-TRAJECTORY VELOCITY ANALYSIS: IMPROVED DERIVATION AND PROOF OF CONCEPT

H. B. Santos, T. A. Coimbra, J. Schleicher, and A. Novais

email: *hbuenos@gmail.com, js@ime.unicamp.br*

keywords: *Remigration, time-migration, migration velocity analysis, seismic velocity interpretation and processing*

ABSTRACT

Remigration trajectories describe the position of an image point in the image domain for different source-receiver offsets as a function of the migration velocity. They can be used for prestack time-migration velocity analysis by means of determining kinematic migration parameters, which in turn, allow to locally correct the velocity model. The main advantage of this technique is that it takes the reflection-point displacement in the midpoint direction into account, thus allowing for a moveout correction for a single reflection point at all offsets of a common image gather (CIG). We have tested the feasibility of the method on synthetic data from three simple models and the Marmousoft data. Our tests show that the proposed tool increases the velocity-model resolution and provides a plausible time-migrated image. The most effort was spent on the event picking, which is critical to the method.

INTRODUCTION

Because of its conceptual clarity and simplicity, residual-moveout (RMO) analysis has become one of the favorite tools for migration velocity analysis (MVA) (Liu and Bleistein, 1995). Many algorithms are based on the moveout formula for a horizontal reflector (Al-Yahya, 1989). Another MVA principle is to follow migrated reflection events through the image domain under variation of the migration velocity (Fomel, 1994; Liptow and Hubral, 1995). It is well known that a single curve in a CMP stacked zero-offset section leads to different reflector images when different migration velocities are used (Figure 1). That is, the image can be thought of as "propagating" as a function of migration velocity (Fomel, 1994), forming a so-called "image wave" (Hubral et al., 1996b).

Remigration, also known as residual migration or velocity continuation, can be seen as a process to construct a seismic image for a refined velocity model from another one already available from a previous migration for a different velocity model (Hubral et al., 1996a; Tygel et al., 1996). In an attempt to achieve more realistic velocity models and migrated images, many residual (or cascaded) methods, as well as remigration processes have been proposed (Rothman et al., 1985; Liptow and Hubral, 1995; Hubral et al., 1996a; Schleicher et al., 1997; Adler, 2003; Fomel, 2003a,b; Schleicher et al., 2008a). Such image-wave remigration procedures can even be extended to anisotropic media (Schleicher and Aleixo, 2007; Schleicher et al., 2008b).

Velocity continuation can be also used on migrated diffractions (Sava et al., 2005; Fomel et al., 2007; Novais et al., 2008) for MVA. Based on velocity continuation, Coimbra et al. (2011, 2012, 2013b) recently introduced a new process of extracting velocity updates for depth migration from the moveout of incorrectly migrated diffraction events by tracing so-called remigration trajectories to their focus point in post-stack migrated images, and Coimbra et al. (2013a) extended their work to the prestack case. This technique makes use of local-slope information extracted from the data with the help of stacks along local trial surfaces. Coimbra et al. (2013c) and Santos et al. (2014) modified this remigration-trajectory MVA method
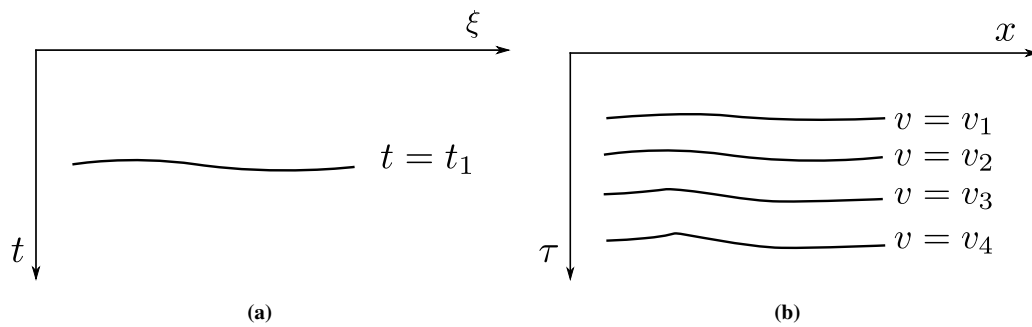
Figure 1: Sketch of: (a) A single reflection event in the time domain and (b) its time migrated images for four different migration velocities.
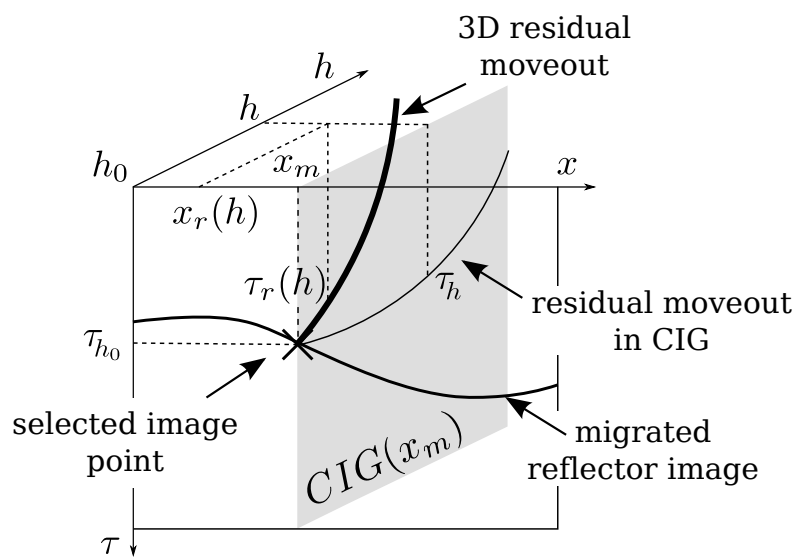
Figure 2: The residual moveout of a dipping reflector in a single CIG at x_m after migration with a wrong velocity is described by curve τ_h (fine line). However, the image of a unique reflection point moves out of the CIG through the whole migrated data volume along a 3D moveout curve $\tau_r(h)$ (bold solid line). This curve can be approximated from information found at point (h_0, x_m, τ_{h_0}). For details, see text.

to make it suitable for an application to time-migration of reflection events in prestack data, presenting an improved derivation of the time-remigration trajectories. In this work, we present an improved derivation of the method's theory as compared to Coimbra et al. (2013c), detail the model-building algorithm, and report on numerical tests of the method applied to synthetic data from three gradient models and to the Marmousoft data. These additional tests confirm the potential of the method to produce plausible velocity-model updates in regions with strong velocity variations.

REMIGRATION TRAJECTORY

The residual moveout of a point on the migrated image of a dipping reflector as a function of half-offset is a three-dimensional curve through the prestack-migrated data volume (see Figure 2). A remigration trajectory describes the position of a point on this moveout curve as a function of migration velocity, considering not only the half-offset, but also the variation of the reflection-point displacement in the midpoint direction (see Figure 3).
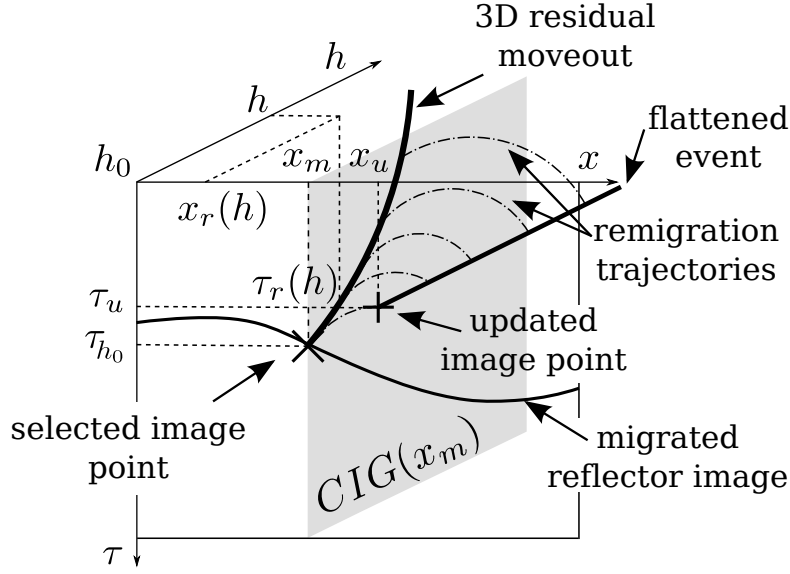
Figure 3: Remigration trajectories (dash-dotted lines) for selected points on the 3D moveout curve (bold solid line) of an incorrectly migrated reflector point (x_m, τ_{h_0}). Also shown is the flattened position of the event at (x_u, τ_u).

Theoretical description

For the mathematical derivation of the remigration trajectory, we start at the well-known fact that a certain reflection point on a dipping reflector is imaged in different common-image gathers (CIGs) at different offsets if the migration velocity is incorrect (Figure 2). Based on the kinematic analysis of velocity continuation, Fomel (2003b) approximated the positioning of the displaced image point up to second order in half-offset h as

$$\tau_r(h, x) = \sqrt{\tau_h^2 - \frac{4(x - x_m)^2}{v_m^2 - v^2} + 4h^2 \left(\frac{1}{v_m^2} - \frac{1}{v^2}\right)},\tag{1}$$

where v is the true average medium velocity and v_m is the (incorrect) migration velocity. Moreover, τ_h is the time coordinate at half-offset h of the image point within the CIG at image position x_m, and $x - x_m$ denotes the relative lateral coordinate, i.e., the distance to the original CIG at x_m (see again Figure 2).

The envelope of these curves at all x determines the lateral displacement x_r as a function of h. This envelope can be determined by setting the derivative with respect to x equal to zero, i.e.,

$$\left.\frac{\partial \tau_r(h, x)}{\partial x}\right|_{x_r} = 0 \,.\tag{2}$$

We find

$$x_r(h) = x_m + \frac{1}{4}\left(v_m^2 - v^2\right)\tau_h D_h \,,\tag{3}$$

where D_h denotes the event dip in the off-CIG or common-offset direction at lateral coordinate x_m and half-offset h. In other words, D_h is given at any h by

$$D_h = \left.\frac{\partial \tau_h}{\partial x}\right|_{x_m} \,.\tag{4}$$

For $h = 0$, equations (1) and (3) reduce to the zero-offset equations derived by Schleicher et al. (1997).

Combining equations (1) and (3), we arrive at the residual-moveout expression as a function of the event dip,

$$\tau_r(h) = \sqrt{\tau_h^2 \left(1 + \frac{v_m^2 - v^2}{4} D_h^2\right) + 4h^2 \left(\frac{1}{v_m^2} - \frac{1}{v^2}\right)} \,.\tag{5}$$

Expressions (3) and (5) together approximately describe the residual moveout of the image of a reflection point in the migrated data volume for a given migration velocity v_m at a given half-offset h (see again Figure 3), if the position τ_h at that offset is known. For not too large offsets, the approximation is valid to the same extend as time migration, i.e., as long as the medium is acceptably described by a locally constant average velocity (which may vary from CIG to CIG). The derivation of more general expressions can be conceived of by using improved approximations for the out-of-CIG displacement (equation (1)).

However, for the use in velocity analysis, equations (3) and (5) together are still insufficient, since they do not allow to predict the continuation from an image point at some half-offset h_0 to the corresponding point at another half-offset h without additional information. For this purpose, we need a relationship between the image-time coordinates τ_{h_0} and τ_h.

To find such a relationship, we start at considering a CMP section for a single reflector below an isotropic constant-velocity overburden with (true) average medium velocity v. At a given reflection point, the conventional NMO traveltimes for two different half-offsets h_0 and h read

$$t_{h_0}^2 = t_0^2 + \frac{4h_0^2}{v_n^2}, \tag{6}$$

$$t_h^2 = t_0^2 + \frac{4h^2}{v_n^2}, \tag{7}$$

where t_{h_0} and t_h are the source-receiver traveltimes, t_0 is the vertical time at zero offset, which is independent of the half-offset h, and v_n is the NMO velocity, used during the processing in a tentative to flatten the events present in the CMP section.

Taking the difference between equations (6) and (7), we find a direct relation between t_{h_0} and t_h that is independent of t_0,

$$t_h^2 = t_{h_0}^2 + \frac{4}{v_n^2}(h^2 - h_0^2). \tag{8}$$

Now, consider time migration using an (incorrect) migration velocity v_m. The traveltime for a source-receiver pair with a half-offset h is defined by the usual double-square-root (DSR) equation,

$$t_h = \sqrt{\frac{\tau_h^2}{4} + \frac{(x_m - \xi + h)^2}{v_m^2}} + \sqrt{\frac{\tau_h^2}{4} + \frac{(x_m - \xi - h)^2}{v_m^2}}, \tag{9}$$

where ξ is the midpoint between source and receiver and, as before, x_m and τ_h are the coordinates of the image point in the time-migrated CIG (Figure 2).

To simplify this expression, we use the fact that for small h, the square roots in equation (9) can be approximated as

$$\sqrt{\frac{\tau_h^2}{4} + \frac{(x_m - \xi \pm h)^2}{v_m^2}} \approx \sqrt{\frac{\tau_h^2}{4} + \frac{(x_m - \xi)^2 + h^2}{v_m^2}} \pm \frac{h(x_m - \xi)}{v_m^2 \sqrt{\frac{\tau_h^2}{4} + \frac{(x_m - \xi)^2 + h^2}{v_m^2}}}. \tag{10}$$

With this approximation, equation (9) can be written for two different half-offsets h and h_0 as

$$t_{h_0} = \sqrt{\tau_{h_0}^2 + 4\frac{(x_m - \xi)^2 + h_0^2}{v_m^2}}, \tag{11}$$

$$t_h = \sqrt{\tau_h^2 + 4\frac{(x_m - \xi)^2 + h^2}{v_m^2}}, \tag{12}$$

Substituting equations (11) and (12) in equation (8) yields the relationship between migrated times τ_{h_0} at h_0 and τ_h at h as

$$\tau_h = \sqrt{\tau_{h_0}^2 + 4(h^2 - h_0^2)\left(\frac{1}{v_n^2} - \frac{1}{v_m^2}\right)}. \tag{13}$$

Another way to reach this relation is to solve the classical expression of Al-Yahya (1989) describing the position of the image of a horizontal reflector in a time-migrated image, viz.,

$$\tau_h = \sqrt{\tau_0^2 + 4h^2 \left(\frac{1}{v^2} - \frac{1}{v_m^2} \right)}, \tag{14}$$

for τ_0 at two half-offsets h and h_0 and equal the results. The advantage of our derivation is that it demonstrates that equation (13) remains valid for a dipping reflector up to second order in h.

It is important to notice that equation (13) is used exclusively to estimate the event position τ_h within the CIG at x_m. The provisional NMO velocity v_n is not needed for any other purpose than fitting the event. Therefore, any expression that reasonably approximates the event can be used instead of equation (13), even without any physical justification.

Equation (13) allows us to estimate the vertical time τ_h at h as a function of τ_{h_0} at h_0 without the need for any information of the zero-offset section. However, we still need the information of the event dip D_h in the migrated volume in the offset direction at all offsets h. To avoid the necessary dip estimations in all involved common-offset migrated sections, we use that the event dip D_h at h is approximately related to the one at h_0 as

$$D_h = D_{h_0} \frac{\tau_{h_0}}{\tau_h}. \tag{15}$$

This relationship is obtained from the derivative of equation (13) with respect to x under the assumption that the variation of v_n can be neglected. It can also be inferred from equation (3) upon noticing that at a fixed h the dislocation $x_r(h) - x_m$ out of the CIG must be the same independently of the initial point of the moveout curve. Note that in agreement with the physics involved, $D_h \to 0$ when $\tau_h \to \infty$.

The set of expressions (3), (5), (13), and (15) describes the so-called remigration trajectory, i.e., the variation of the position of each point on the 3D residual moveout in the 3D migrated data volume as a function of the migration velocity v_m (see Figure 3). With this trajectory, we can estimate whereto in the data volume a point (h_0, τ_{h_0}) in a CIG will move when the migration velocity is changed. When applying this equation to all points in a CIG at a chosen image point, we can estimate the velocity value for which the resulting set of moved points becomes closest to a horizontal line.

To calculate the image-point positions with this set of equations, we need an estimate of all image times τ_h in the initial CIG and all event dips D_h perpendicular to the CIG. For the estimation of τ_h, we fit a curve of the form of equation (13) to the migrated event within the CIG at x_m. To estimate the local slopes D_h in all common-offset migrated sections at each h, we use a generalization of local slant stacks. Upon the use of equation (15), we define a surface $T = T(h, x)$ as

$$T(h, x) = \tau_h + (x - x_m)D_h = \tau_h + (x - x_m)\frac{\tau_{h_0}}{\tau_h}D_{h_0}. \tag{16}$$

This surface is composed of all tangent lines to the event surface in the migrated data volume, if the correct value of D_{h_0} is used. This fact can be used to estimate this parameter from the date by semblance maximization using trial surfaces. Since the estimate employs a surface rather than a line stack, it provides more reliable results.

Velocity analysis

With the remigration trajectory established, we can now devise a migration-velocity-analysis algorithm based on local-slope estimation and approximate image-wave propagation of the CIG. For the purpose of velocity analysis, the residual moveout of the remigration trajectory must be minimized, since at the correct velocity, the event in the CIG must be horizontal. Therefore, we can choose the derivative of $\tau_r(h)$ as the objective function. Thus, the optimization condition is

$$\min_v \left\| \frac{\partial \tau_r}{\partial h} \right\|. \tag{17}$$

In this paper, we minimize this derivative analytically using an exhaustive search. For this purpose, we use the time position τ_{h_0} and the slope parameter D_{h_0} extracted from the data to calculate the remigration

trajectory according to equation (5) with the help of equation (13). Doing so for a reasonable set of migration velocities allows us to look for the velocity value that produces the lowest variation of τ_r as a function of h. This procedure turned out to be faster than an optimization process using Newton's method.

The minimum value of the variation of τ_r as a function of h defines the desired updated time-migration velocity v_u associated with the image point at (x_m, τ_{h_0}). For velocity building, v_u is attributed to its updated position (x_u, τ_u), determined equations (3) and (5) upon the use of v_u instead of v (see again Figure 3).

MODEL BUILDING ALGORITHM

To construct the final velocity model, we propose to use the above corrections in an iterative process. The information contained in a CIG at a selected migrated reflection point allows to construct the approximate time-remigration trajectory, which then provides an update for the velocity value and the spacial and time coordinates of that point. The algorithm for this procedure and the corresponding flowchart are detailed in Figure 4.

Let us emphasize again that velocity v_n (equation (13); step (3)) is a provisional velocity estimate that is used only to determine the values of τ_h in the current CIG at point (x_m, τ_{h_0}). In turn, these values of τ_h are used to flatten the event along the remigration trajectory (equation (3) and (5); step (7)) by minimization of the residual moveout (equation (17); step (8)), which then determines the updated migration velocity v.

By its principle, the proposed MVA algorithm is a *local* procedure, updating the velocity at a single image point at a time. If sufficient image points are available in a certain region, a smooth model can be interpolated for that region. In the interpolation stage, a-priori information or constraints can be taken into account. In our numerical tests on synthetic data, reported below, the method was able to build time-migration velocity models without an initial model, starting with a constant-velocity migration, as long as the model complexity lies within the validity range of time migration.

NUMERICAL EXAMPLES

We have applied our time remigration technique to three constant-gradient velocity models with sets of dipping reflectors, and the more complex Marmousoft data set.

Application to constant-gradient models

We applied the method to three constant-gradient models that can be thought of as representing subregions of a larger model. To verify the feasibility of our method, which was derived under the assumption of constant average velocities, in more realistic situations, we chose rather strong velocity gradients in the vertical, horizontal, and diagonal directions. The true velocity models are given by

$$v(z) \quad = \quad 2000 + 0.5z \text{ m/s} , \tag{18}$$

$$v(x) \quad = \quad 2000 + 0.5x \text{ m/s} , \tag{19}$$

$$v(x, z) \quad = \quad 2000 + 0.5x + 0.5z \text{ m/s} . \tag{20}$$

All three models contain six interfaces with, from top to bottom, initial depths at the origin of 400 m, 500 m, 600 m, 700 m, 800 m, and 900 m, and dips of $0°$, $4.8°$, $10°$, $15°$, $23.6°$, $39.5°$, respectively. Moreover, they contain seven diffraction points in different parts of the models. The diffraction events were not used for velocity analysis. Their only purpose is the quality control of the extracted velocity models.

We generated the corresponding synthetic data sets using a Kirchhoff-modeling algorithm of Seismic Un*x (Cohen and Stockwell, 2014). We simulated 25 common-offset sections for offsets between 200 m and 680 m spaced at 20 m, with a sampling rate of 2 ms up to a maximum time of 2.5 s, each with 400 source-receivers pairs spaced at 10 m between CMP coordinates 500 m and 4500 m, thus covering an extension of 4000 m. We used a symmetric Ricker wavelet with 20 Hz peak frequency, and contaminated the data with pseudo-random Gaussian noise with zero mean and at level of 5% of the maximum amplitude.

We then applied the present remigration-trajectory MVA method to these data. The first step consisted in a constant-velocity time migration. For these examples, we used an intermediate velocity of $v_0 = 3.0$ km/s.

ALGORITHM

1. Time migration of the data with a given initial velocity model $v_m = v_m(x, \tau)$. In our numerical tests, a constant-velocity migration was sufficient to start the process.

2. Selection of an image point (x_m, τ_{h_0}) in the shortest-offset migrated section or stacked migrated image. Normally, it is useful to choose points on already visible reflector images. In our numerical examples, we chose the points by visual inspection. Automatic picking might be an option, but weak reflector amplitudes, usually discarded by automatic picking procedures, often indicate the need for velocity improvements.

3. Coherence analysis in the CIG at (x_m, τ_{h_0}) using equation (13) for a consistent range of NMO velocities v_n. The maximum coherence value defines a (temporary) NMO velocity v_n that best describes the event at all half-offsets h.

4. Computation of τ_h for all h using equation (13) with the so-determined v_n and the current migration velocity v_m.

5. Estimation of the off-CIG dip D_{h_0} by means of a coherence analysis along the surface defined by equation (16).

6. Computation of D_h for all h using equation (15).

7. Calculation of several remigration trajectories using equations (3) and (5) for a range of velocities v. In our numerical tests, this range had to be finer sampled than the above one for v_n.

8. Determination of the updated migration velocity v_u for (x_m, τ_{h_0}) that minimizes the variation of τ_r in the offset direction, according to equation (17).

9. Calculation of the corrected position (x_u, τ_u) of the selected image point.

10. Loop over steps (2) to (8) until a sufficient number of image points are processed.

11. Interpolation of the set of new velocity values.

12. Model smoothing if necessary. In some of our numerical tests, a moving average filter turned out to be useful to improve the correlation between adjacent image points.

13. Time migration of the original data with the new velocity model.

14. Loop over steps (2) to (13) until the events in all CIGs are satisfactorily flattened.
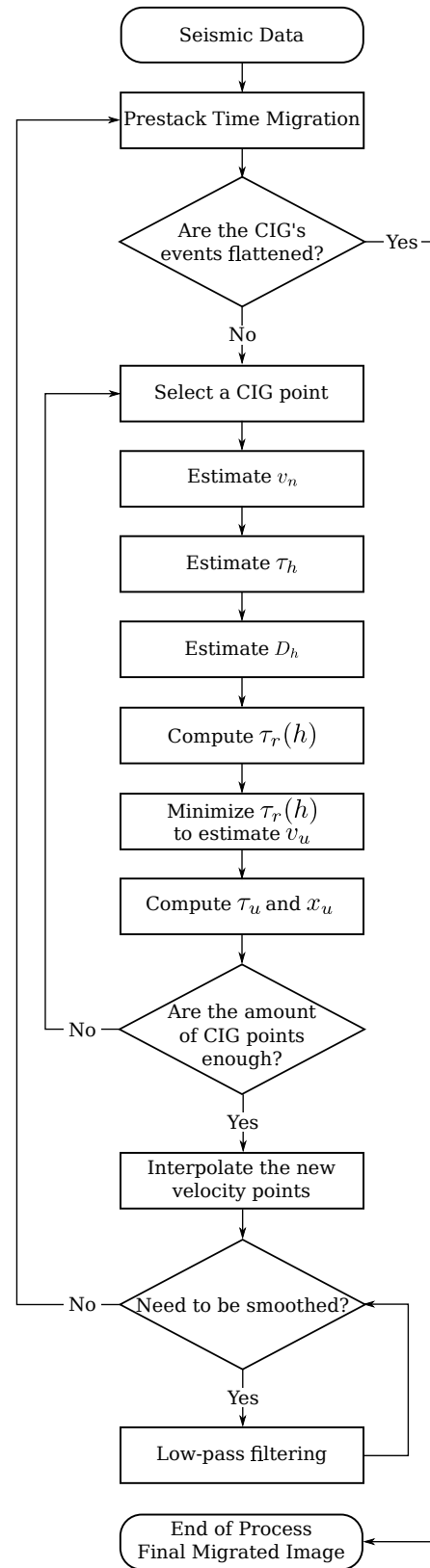
Figure 4: Remigration-trajectory MVA. Left: Algorithm. Right: Flowchart.

(a)

(b)
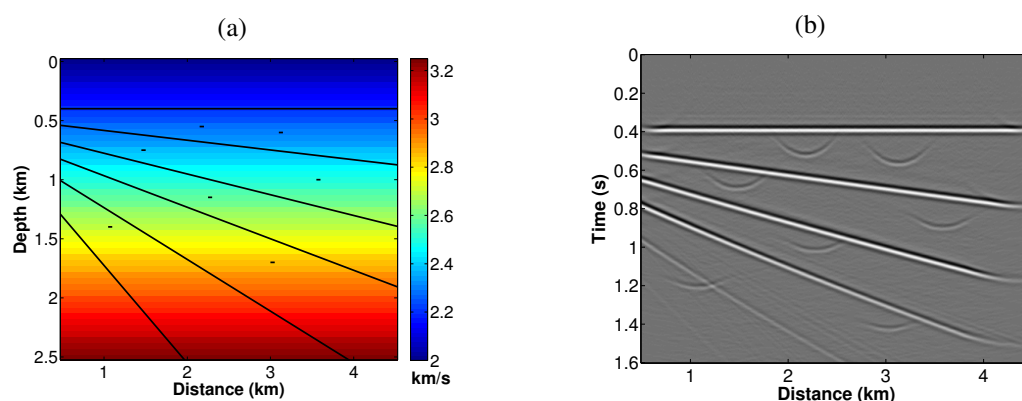
Figure 5: Vertical-gradient model: (a) Velocity model with reflectors and control diffractors. (b) Time-migrated image using $v_0 = 3.0$ km/s.

(a)

(b)

(c)

(d)
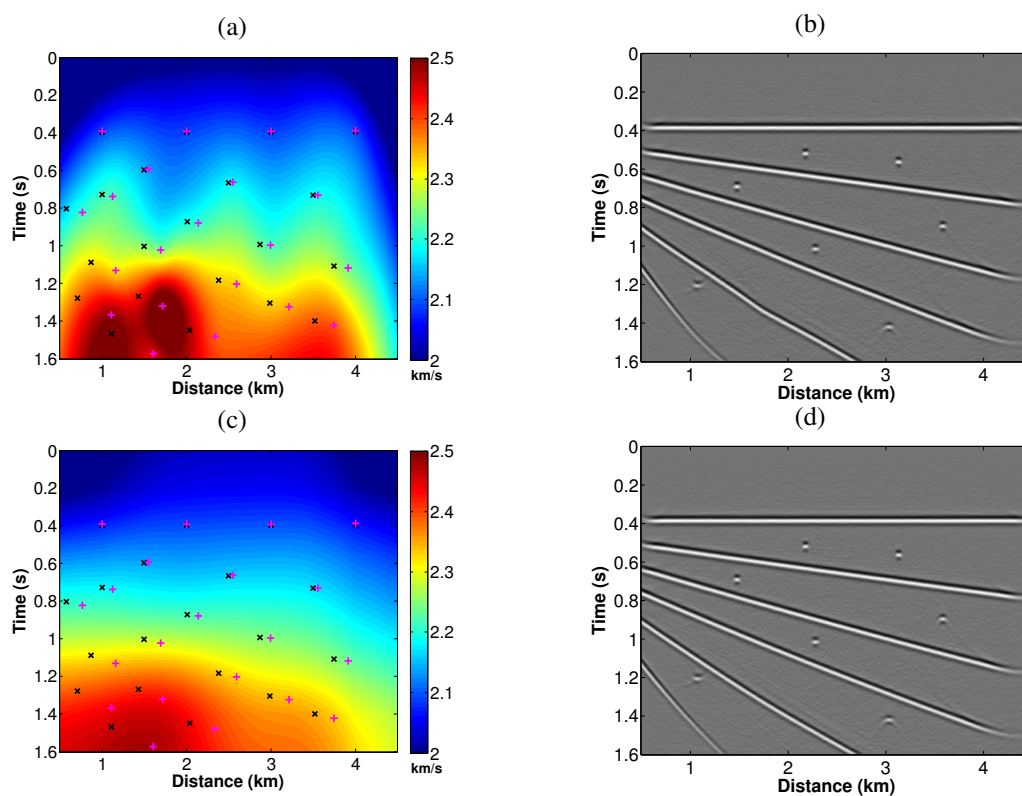
Figure 6: Vertical-gradient model: (a) Extracted velocity model after one iteration with 21 image points and (b) corresponding final time-migrated image. (c) Extracted velocity model after moving-average smoothing and (d) corresponding final time-migrated image. Also shown in parts (a) and (c) are the picked image points (black crosses) and their updated positions (pink plusses).

Figures 5 to 7 summarize the results for the vertical-gradient model. Figure 5a depicts the true velocity model with reflectors and control diffractors, and Figure 5b shows the time-migrated zero-offset section using a constant migration velocity of 3000 m/s.

From this initial migration, we started the remigration-trajectory velocity analysis. To investigate the quality of the result in dependence of the number of points picked, we performed the analysis twice, once with 21 image points and once with 100 image points. Figure 6a shows the 21 image points picked in the first run (black crosses) together with their updated positions (pink plusses) superimposed over the
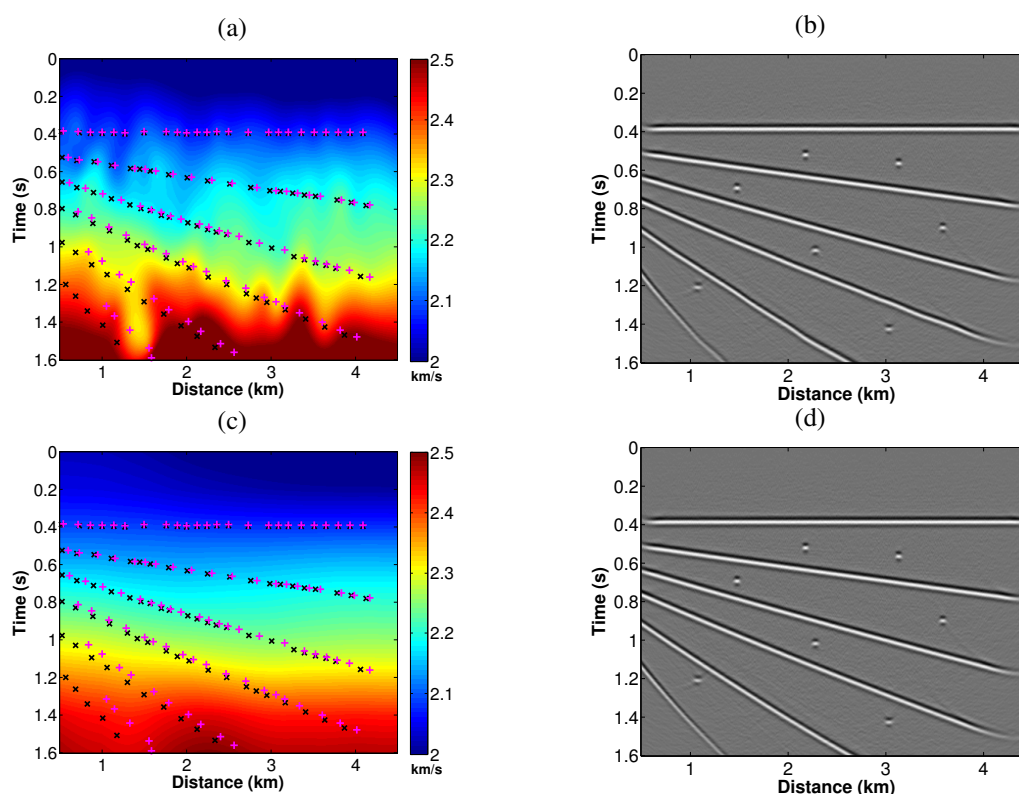
Figure 7: Vertical-gradient model: (a) Extracted velocity model after one iteration with 100 image points and (b) corresponding final time-migrated image. (c) Extracted velocity model after moving-average smoothing and (d) corresponding final time-migrated image. Also shown in parts (a) and (c) are the picked image points (black crosses) and their updated positions (pink plusses).

obtained updated velocity model after one iteration. This model results from a B-splines interpolation (Matlab implementation, see Sandwell, 1987) of the updated velocities at the 21 updated image-point locations. Figure 6b shows the corresponding time-migrated stacked section. In the velocity model, we recognize some undulations, indicating that the velocity estimate is better at the chosen image points than in their vicinity. Nonetheless, the control diffractors in the image are reasonably focused and the reflectors only slightly curved. This indicates that the model in Figure 6a already is an acceptable time-migration velocity model. For further improvement, we applied two passes of moving-average smoothing with a 1 km × 0.4 s (100 by 100 points) window. The idea is to carry the velocity information at the chosen image points over to their vicinities where no updated velocity values are available. Figures 6c and d show the so-obtained model and the corresponding image. While the model has improved and resembles the true model of Figure 5a more closely, the time-migrated image of Figure 6d is almost identical to that of Figure 6b.

Figure 7a shows the 100 image points picked in the second test (black crosses), also together with their updated positions (pink plusses) and superimposed over the obtained updated velocity model after one iteration. Again, Figure 7b shows the corresponding time-migrated stacked section. In comparison to Figure 6a, we observe that the velocity undulations in Figure 7a are reduced in amplitude and wavelength. The migrated image in Figure 7b has slightly improved as compared to Figure 6b, particularly regarding the positioning of the deepest reflector and the focusing of the deepest diffractor. Moving-average smoothing further improves the model (Figure 7c), but again has little effect on the resulting image (Figure 7d).

Similar conclusions can be drawn from the corresponding experiments with the horizontal (Figures 8, 9, and 10) and diagonal (Figures 11, 12, and 13) gradients. While the models extracted with 100 image points (Figures 10a and 13a) are slightly better than the ones extracted with 21 image points (Figures 9a and 12a), it is doubtful that the improvements warrant fivefold picking expense. The smoothed models
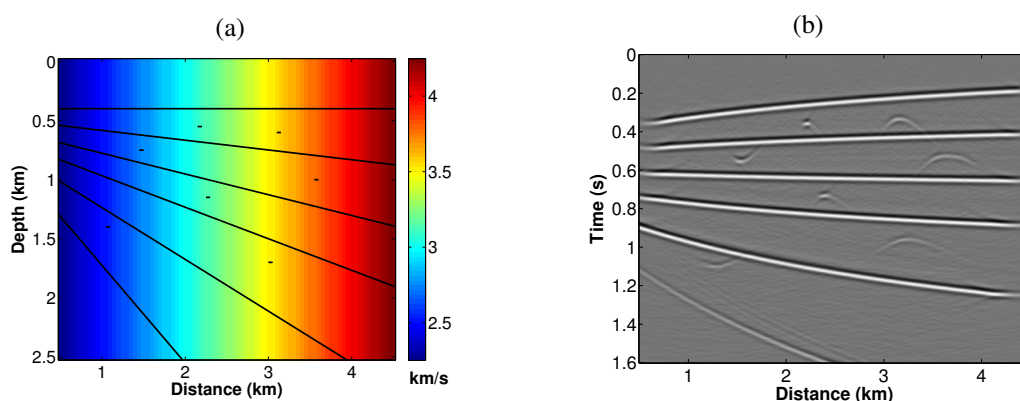
Figure 8: Horizontal-gradient model: (a) Velocity model with reflectors and control diffractors. (b) Time-migrated image using $v_0 = 3.0$ km/s.
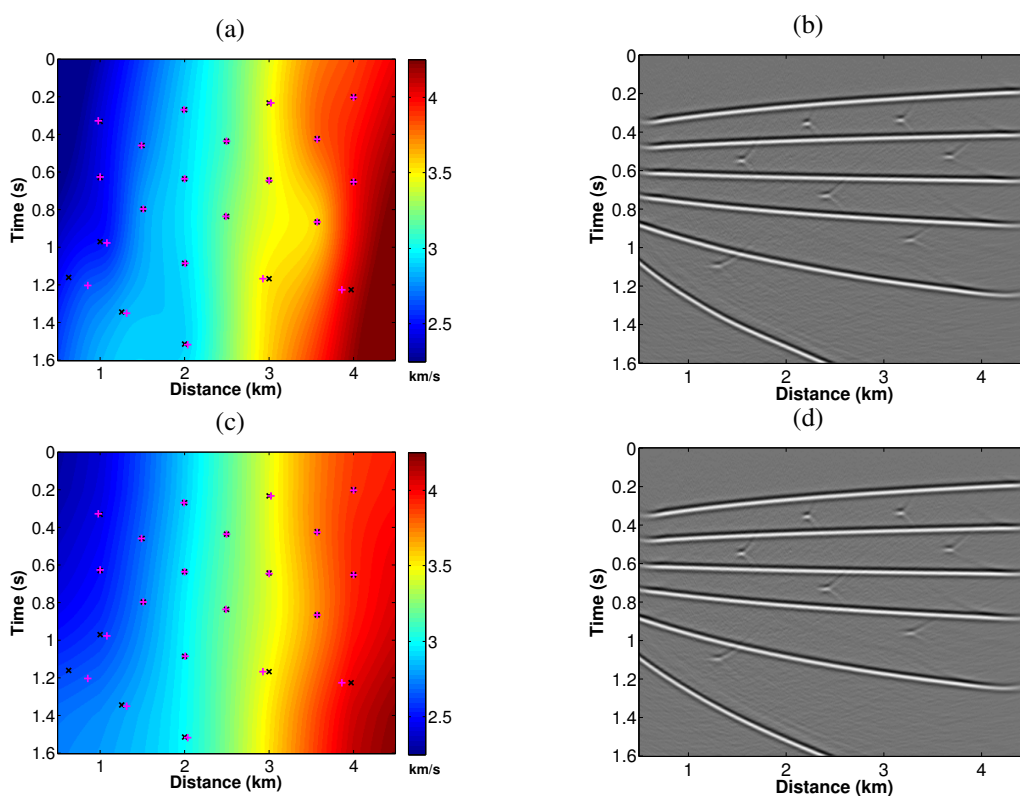
Figure 9: Horizontal-gradient model: (a) Extracted velocity model after one iteration with 21 image points and (b) corresponding final time-migrated image. (c) Extracted velocity model after moving-average smoothing and (d) corresponding final time-migrated image. Also shown in parts (a) and (c) are the picked image points (black crosses) and their updated positions (pink plusses).

using 21 points (Figures 9c and 12c) almost reach the same quality as the ones obtained with 100 points (Figures 10c and 13c).

These tests demonstrate that even in the presence of a strong velocity gradient, the method is capable of extracting meaningful time-migration velocity models using a not too large number of image points where reflector images can be picked in the incorrectly migrated image.
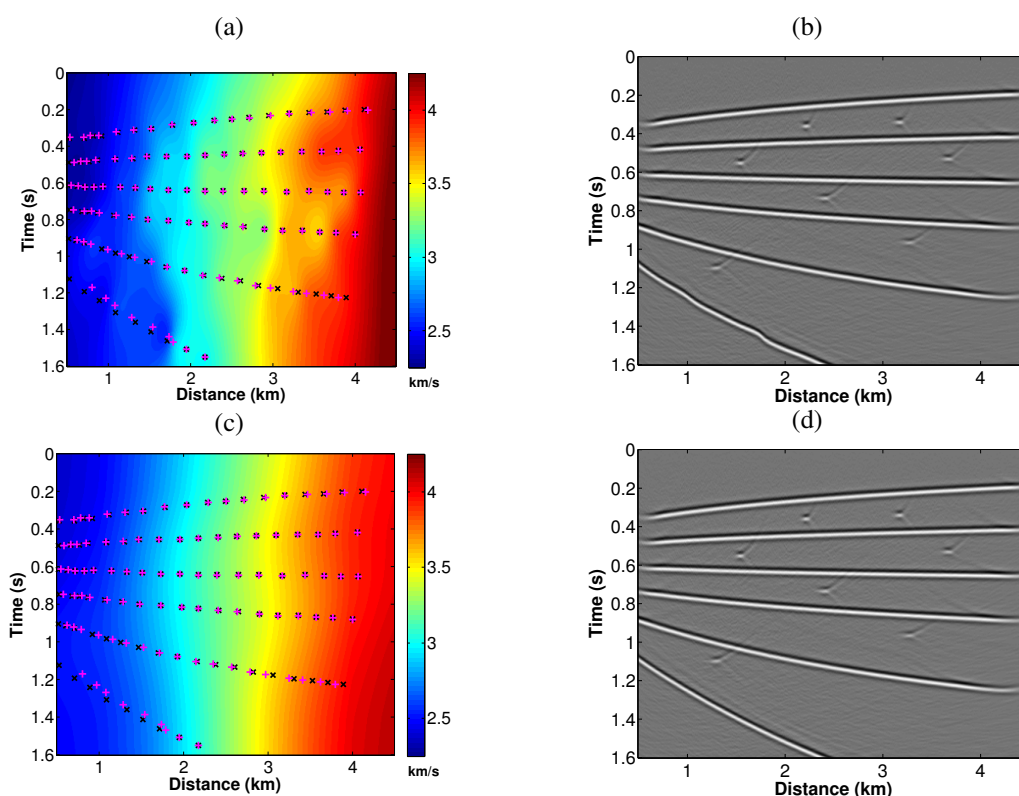
Figure 10: Horizontal-gradient model: (a) Extracted velocity model after one iteration with 100 image points and (b) corresponding final time-migrated image. (c) Extracted velocity model after moving-average smoothing and (d) corresponding final time-migrated image. Also shown in parts (a) and (c) are the picked image points (black crosses) and their updated positions (pink plusses).
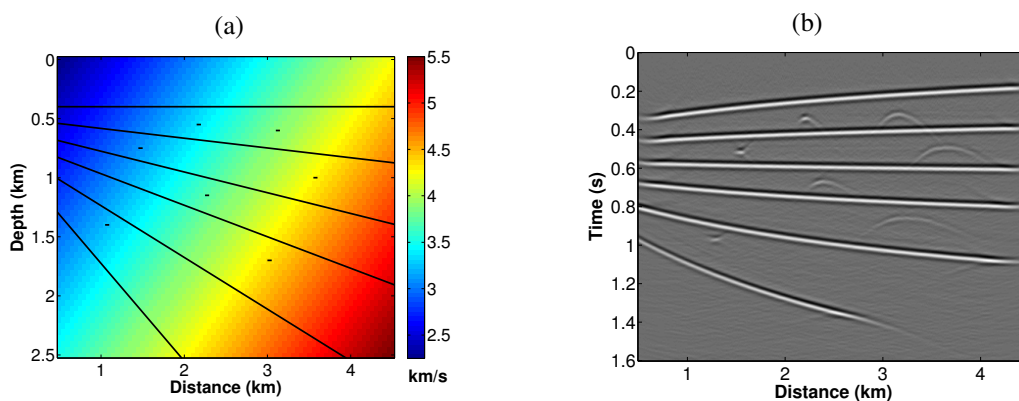
Figure 11: Diagonal-gradient model: (a) Velocity model with reflectors and control diffractors. (b) Time-migrated image using $v_0 = 3.0$ km/s.

Application to the Marmousoft data

Encouraged by these results, we set out for a more realistic test. We applied the described MVA technique to the Marmousoft data (Billette et al., 2003). These data were constructed by Born modeling in a smoothed version of the Marmousi model. The true (depth) Marmousoft velocity model is depicted in Figure 14a. We chose this model so as to analyze the behaviour of our MVA method in a complex sedimentary geology. We did not expect the method to work in the central part of the model because of the limits of time migration.

(a)   (b)

(e)   (d)
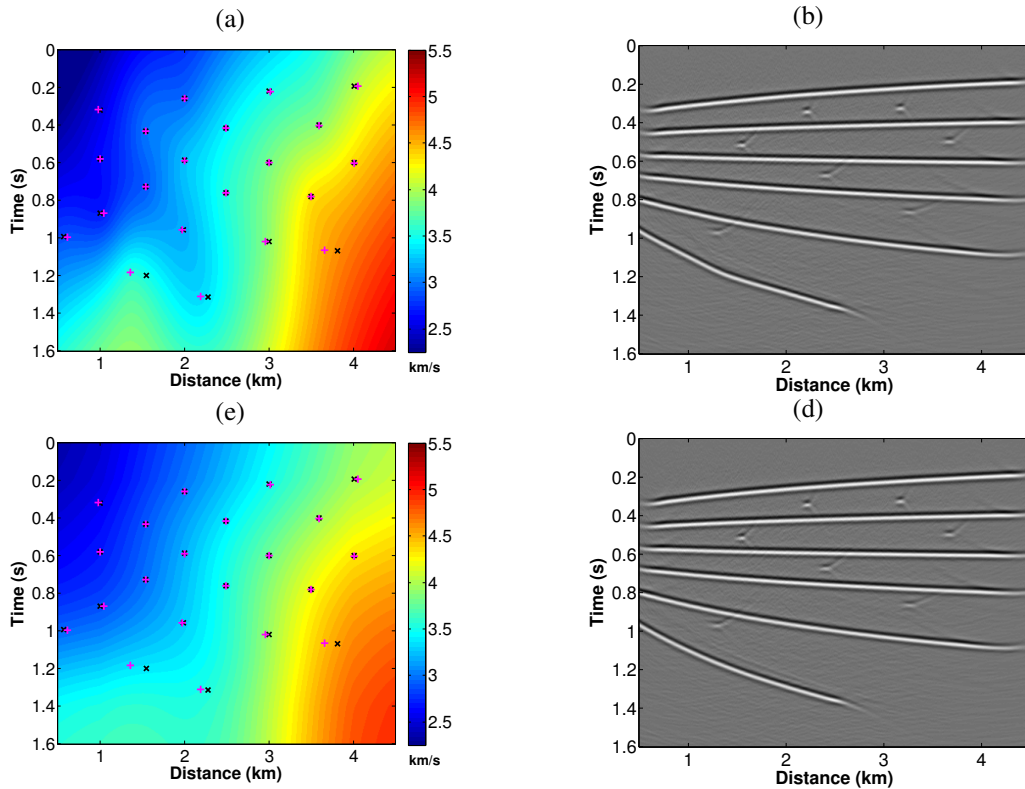
Figure 12: Diagonal-gradient model: (a) Extracted velocity model after one iteration with 21 image points and (b) corresponding final time-migrated image. (c) Extracted velocity model after moving-average smoothing and (d) corresponding final time-migrated image. Also shown in parts (a) and (c) are the picked image points (black crosses) and their updated positions (pink plusses).

In order to simulate a time-migration velocity model we computed the root-mean-square (v_{rms}) velocity model in pseudo-time from the stratigraphic velocity using vertical conversion only. The resulting time-velocity model is depicted in Figure 14b. It indicates acceptable migration velocity values, though probably laterally mispositioned.

The Marmousoft data contain traces at every 25 meters with a sampling rate of 4 ms. We used 96 common-offset sections with source-receiver offsets between 100 m and 2475 m. Figure 15a shows a short-offset section with a total source-receiver offset of 100 m.

To these data, we applied the remigration-trajectory MVA method. For the first migration, we chose $v_0 = 2.0$ km/s. Figure 15b depicts the migrated image obtained from the short-offset data of Figure 15a. The migration aperture used was 241 traces.

Next, we picked 70 points on some of the most prominent migrated events in the image of Figure 15b. At the positions of these picks, we extracted local slopes in the migrated common-offset section and then minimized the residual moveouts along the remigration trajectories as described above. Figure 15c shows the locations of our picks (black crosses) and their corrected positions after velocity updating (pink plusses) overlain on the resulting updated velocity model. As before, we used B-splines to interpolate the velocity model in the complete region.

We then used the velocity model of Figure 15c for a second migration. The result is depicted in Figure 15d. We recognize that the updated velocity model leads to an improved migrated image, particularly regarding the upper parts of the fault lines and the reflectors in the sedimentary regions on both sides of the model.

To eliminate the unrealistic oscillations in the velocity model, we smoothed it (Figure 15c) by two passes of a moving average with a 2.5 km×0.4 s (100 by 100 points) window (see Figure 15e). The Kirchhoff-migrated image corresponding to this velocity model is depicted in Figure 15f.
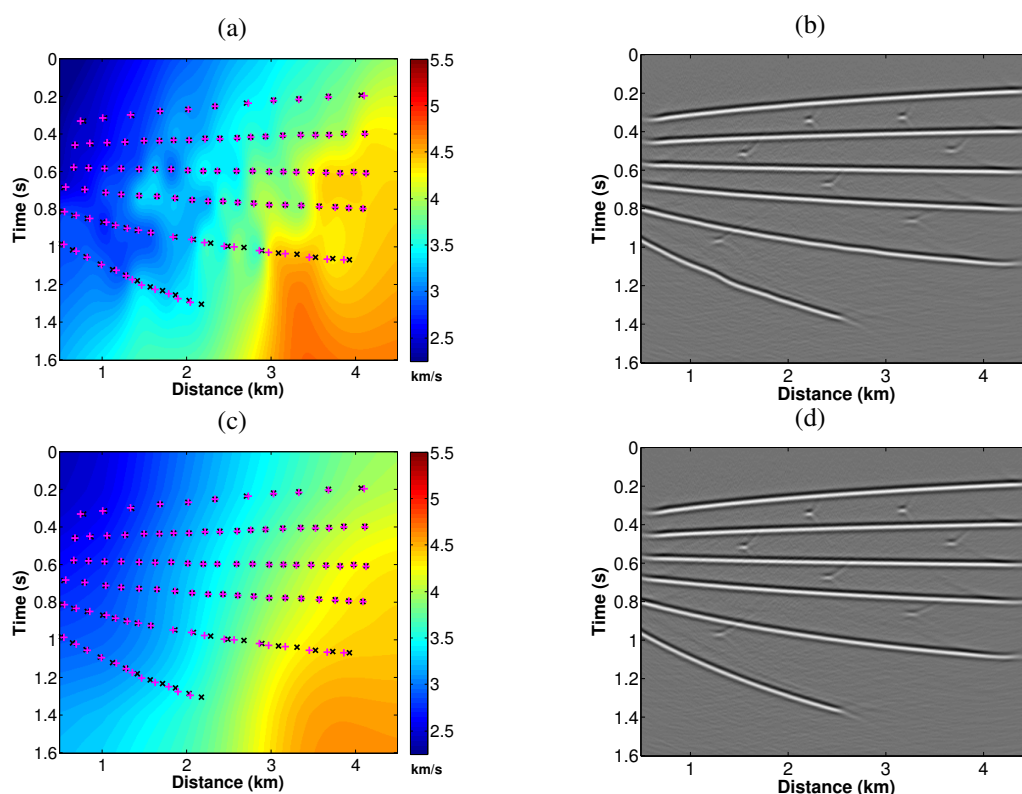
Figure 13: Diagonal-gradient model: (a) Extracted velocity model after one iteration with 100 image points and (b) corresponding final time-migrated image. (c) Extracted velocity model after moving-average smoothing and (d) corresponding final time-migrated image. Also shown in parts (a) and (c) are the picked image points (black crosses) and their updated positions (pink plusses).
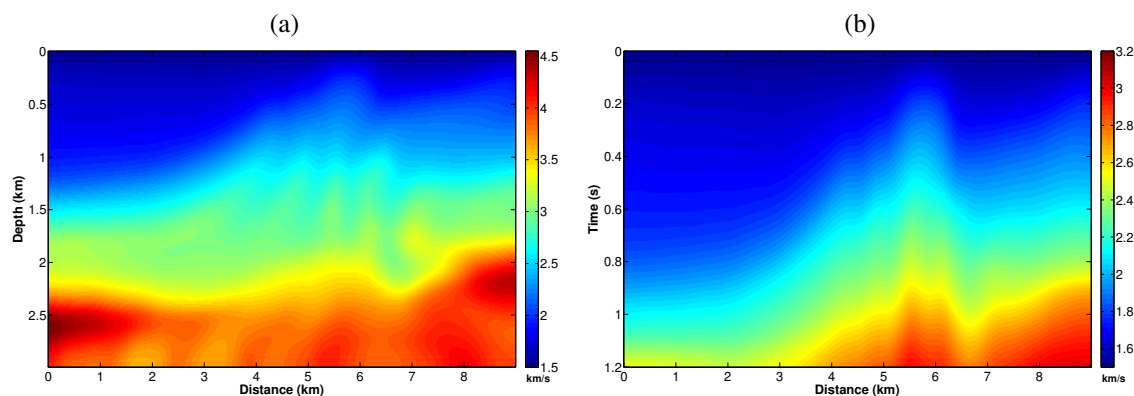
Figure 14: Marmousoft velocity models. (a) Depth velocity model (Billette et al., 2003). (b) Time-velocity model computed from (a) by vertical depth-to-time conversion.

Although the velocity models of Figures 15c and e are rather different, the corresponding migrated images (Figures 15d and f) are quite similar, indicating that both velocity models are equivalent regarding the final time-migration result. These results are in agreement with those produced by common-image gather image-wave propagation and double multi-stack migration (see Santos et al. (2013a) and Santos et al. (2013b) for a parameterization discussion). For further evaluation of the model quality, a time-to-depth conversion will be necessary to compare the attainable model quality as well as to check its application as an initial model for tomographic or depth MVA methods.
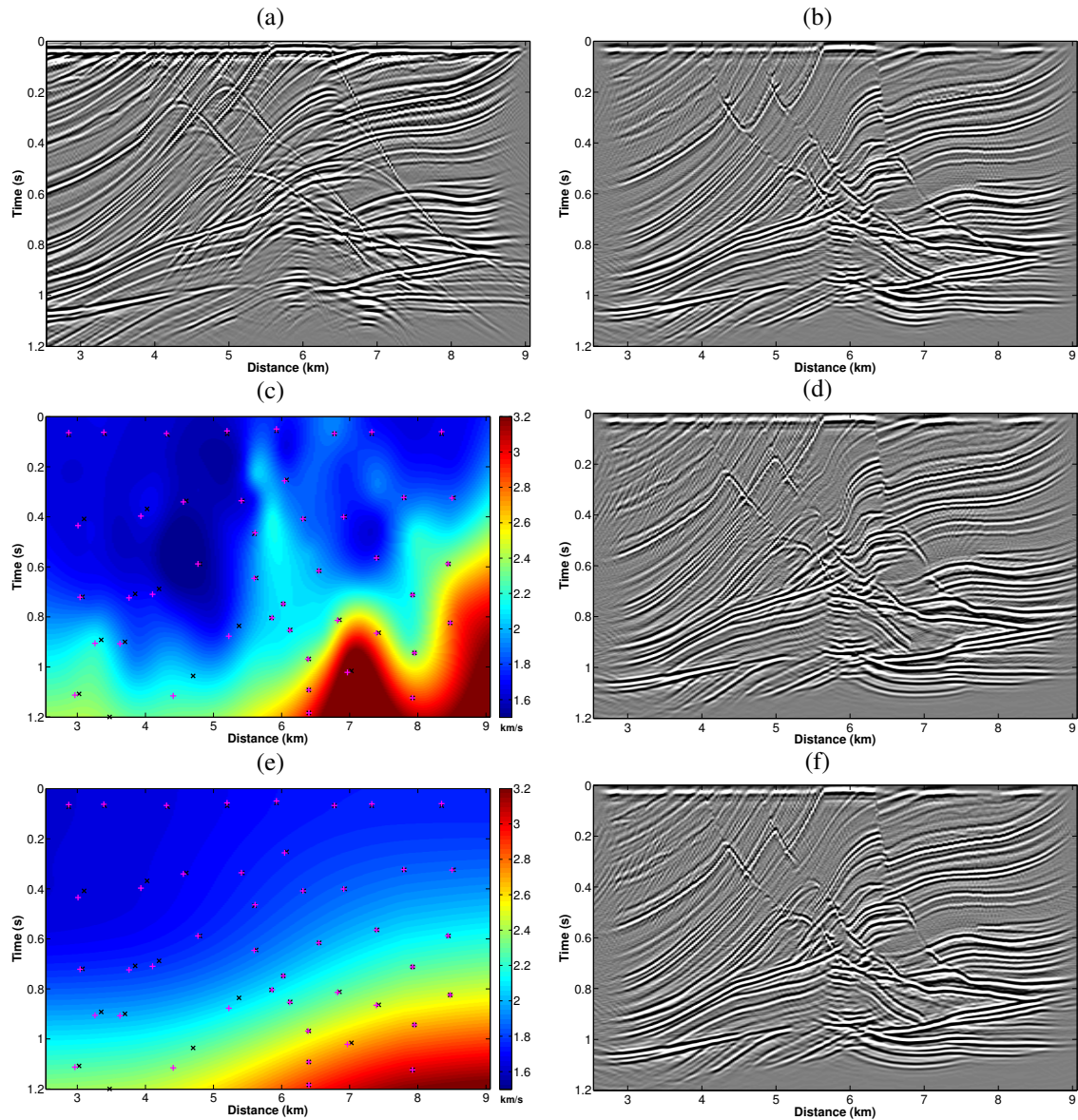
Figure 15: Single iteration of remigration-trajectory MVA on the Marmousoft data. (a) Seismic near-offset section. (b) Time-migrated image of the seismic near-offset section using a constant velocity $v_0 = 2$ km/s and migration aperture equal to 141 traces. (c) Extracted velocity model after one iteration. Also shown are the 70 picked image points (black crosses) and their updated positions (pink plusses). (d) Final time-migrated image by a migration aperture equal to 241 traces. (e) and (f) show the results after moving-average smoothing by two passes with a 2.5 km×0.4 s (100 by 100 points) window.

CONCLUSIONS

We have investigated an MVA tool that uses the estimation of local kinematic attributes of selected events in seismic data to update the velocity model and improve the positioning of key reflectors. The method is based on image-wave propagation in the common-image-gather (CIG) domain described by the means of time-remigration trajectories in the prestack time-migrated domain. Such a trajectory is defined as the set of points where a certain point on a reflection event is migrated to as a function of migration velocity.

The method consists of analyzing the local slope of selected key reflections and determining the velocity value for which an approximate residual-moveout (RMO) expression is minimized. The advantage of this

procedure over conventional MVA methods is that the RMO expression follows the events outside a fixed CIG. In this paper, we have provided an improved theoretical derivation, a detail algorithm for the method's implementation, and additional numerical tests. In these tests, the method led to acceptable time-migration velocity models in a single iterations, even if the starting model was simply a constant velocity. Also the sedimentary shallow part of the Marmousoft model was satisfactorily resolved in one iterations. Tests with different numbers of picked event points demonstrated that the number of points does not need to be very large. Our results indicated that a step of smoothing the data can be helpful, especially for deeper and/or steeper events.

The computational cost of the technique is determined by the cost of prestack time migration in each iteration. Intermediate computations are negligible. The most human effort was spent on the event picking, which is critical to the method. The rather low number of image points needed was helpful to reduce turnaround time. Future research will have to show if this picking process can be automatized, so that the number of picks will no longer be a restrictive parameter.

By its principle, the proposed MVA algorithm is a *local* procedure, updating the velocity at a single image point at a time. If sufficient image points are available in a certain model region, a smooth velocity distribution can be interpolated for that region. In the interpolation stage, a-priori information or constraints can be taken into account. In our numerical tests on synthetic data, we applied the method to simple models consisting of a single region in order to study its behaviour under different conditions. The simple models could be inverted in a single iteration.

We believe that the method's main application will be in the local improvement of previously existing velocity models to enhance the focusing of selected key horizons. Further research will be necessary to extend the method to depth MVA.

REFERENCES

Adler, F. (2003). Kirchhoff image propagation. *Geophysics*, 67(1):126–134.

Al-Yahya, K. M. (1989). Velocity analysis by iterative profile migration. *Geophysics*, 54(06):718–729.

Billette, F., Le Bégat, S., Podvin, P., and Lambaré, G. (2003). Practical aspects and applications of 2D sterotomography. *Geophysics*, 68(3):1008–1021.

Cohen, J. K. and Stockwell, J. J. W. (2014). CWP/SU: Seismic Un*x Release No. 43R6: An open source software package for seismic research and processing. *Center for Wave Phenomena, Colorado School of Mines*.

Coimbra, T. A., de Figueiredo, J. J. S., Novais, A., and Schleicher, J. (2011). Migration velocity analysis with diffraction events using residual moveout. *Annual WIT report*, 15:57–70.

Coimbra, T. A., de Figueiredo, J. J. S., Novais, A., Schleicher, J., and Arashiro, S. (2013a). Migration velocity analysis using residual diffraction moveout in the pre-stack depth domain. *Annual WIT report*, 17:44–53.

Coimbra, T. A., de Figueiredo, J. J. S., Schleicher, J., Novais, A., and Costa, J. (2013b). Migration velocity analysis using residual diffraction moveout in the poststack depth domain. *Geophysics*, 78(3):S125–S135.

Coimbra, T. A., de Figueiredo, J. J. S., Schleicher, J., Novais, A., and Costa, J. C. (2012). Migration velocity analysis with diffraction events using residual moveout: Application to SIGSBEE 2B data. *Annual WIT report*, 16:45–58.

Coimbra, T. A., Santos, H. B., Schleicher, J., and Novais, A. (2013c). Prestack migration velocity analysis using time-remigration trajectories. *Annual WIT report*, 17:66–79.

Fomel, S. (1994). Method of velocity continuation in the problem of seismic time migration. *Russian Geology and Geophysics*, 35(5):100–111.

Fomel, S. (2003a). Time migration velocity analysis by velocity continuation. *Geophysics*, 68(5):1662–1672.

Fomel, S. (2003b). Velocity continuation and the anatomy of residual prestack time migration. *Geophysics*, 67(5):1650–1661.

Fomel, S., Landa, E., and Taner, M. T. (2007). Poststack velocity analysis by separation and imaging of seismic diffractions. *Geophysics*, 72(6):U89–U94.

Hubral, P., Schleicher, J., and Tygel, M. (1996a). A unified approach to 3-D seismic reflection imaging - Part I: Basic concepts. *Geophysics*, 61:742–758.

Hubral, P., Tygel, M., and Schleicher, J. (1996b). Seismic image waves. *Geophysical Journal International*, 125:431–442.

Liptow, F. and Hubral, P. (1995). Migrating around in circles. *The Leading Edge*, 14(11):1125–1127.

Liu, Z. and Bleistein, N. (1995). Migration velocity analysis: Theory and an iterative algorithm. *Geophysics*, 60(1):142–153.

Novais, A., Costa, J., and Schleicher, J. (2008). GPR velocity determination by image-wave remigration. *Journal of Applied Geophysics*, 65(2):65–72.

Rothman, D., Levin, S., and Rocca, F. (1985). Residual migration: Applications and limitations. *Geophysics*, 50(1):110–126.

Sandwell, D. T. (1987). Biharmonic spline interpolation of GEOS-3 and SEASAT altimeter data. *Geophysical Research Letters*, 2:139–142.

Santos, H. B., Coimbra, T. A., Schleicher, J., and Novais, A. (2014). Prestack time-migration velocity analysis using remigration trajectories. *Geophysics*. Submitted.

Santos, H. B., Schleicher, J., and Novais, A. (2013a). Initial-model construction for MVA techniques. In *Expanded Abstracts, 75th EAGE Conference & Exhibition*. EAGE Publications BV.

Santos, H. B., Schleicher, J., and Novais, A. (2013b). Initial-model construction for MVA techniques. *Annual WIT report*, 17:124–135.

Sava, P., Biondi, B., and Etgen, J. (2005). Wave-equation migration velocity analysis by focusing diffractions and reflections. *Geophysics*, 70(3):U19–U27.

Schleicher, J. and Aleixo, R. (2007). Time and depth remigration in elliptically anisotropic media using image-wave propagation. *Geophysics*, 72:S1–S9.

Schleicher, J., Costa, J. C., and Novais, A. (2008a). Time-migration velocity analysis by image-wave propagation of common-image gathers. *Geophysics*, 73(5):VE161–VE171.

Schleicher, J., Hubral, P., and Höcht, G. (1997). Seismic constant-velocity remigration. *Geophysics*, 62(2):589–597.

Schleicher, J., Novais, A., and Costa, J. C. (2008b). Vertical image waves in elliptically inhomogeneous media. *Studia Geophysica et Geodaetica*, 52(1):101–122.

Tygel, M., Schleicher, J., and Hubral, P. (1996). A unified approach to 3-D seismic reflection imaging - Part II: Theory. *Geophysics*, 61:759–775.